Journal of the Serbian Chemical Society
JSCS@tmf.bg.ac.rs • www.shd.org.rs/JSCS
J. Serb. Chem. Soc. *89* (12) 1571–1585 (2024)
JSCS–5807
Original scientific paper
Published 26 December, 2024

Sustainable synthesis of samarium molybdate nanoparticles: a simple electrochemical tool for detection of environmental pollutant metol

TIJANA MUTIĆ[1], VESNA STANKOVIĆ[1], JADRANKA MILIKIĆ[2], DANICA BAJUK-BOGDANOVIĆ[2], KURT KALCHER[3], ASTRID ORTNER[4], DRAGAN MANOJLOVIĆ[5] and DALIBOR STANKOVIĆ[5]*

[1]University of Belgrade, Institute of Chemistry, Technology and Metallurgy, National Institute of the Republic of Serbia, Njegoševa 12, 11000 Belgrade, Serbia, [2]University of Belgrade, Faculty of Physical Chemistry, Studentski trg 12–16, 11158 Belgrade, Serbia, [3]Institute of Chemistry, Analytical Chemistry, Karl-Franzens University, Universitaetsplatz I/I, 8010 Graz, Austria, [4]University of Graz, Institute of Pharmaceutical Sciences, Department of Pharmaceutical Chemistry, Schubertstraße 1, 8010 Graz, Austria and [5]University of Belgrade, Faculty of Chemistry, Studentski Trg 12–16, 11158 Belgrade, Serbia

(Received 13 September, revised 7 October, accepted 2 December 2024)

Abstract: This study focused on creating a highly effective sensor for detecting and quantifying the nitrogen-organic pollutant metol (MTL). For this purpose, samarium molybdate ($Sm_2(MoO_4)_3$) nanoparticles were synthesized using an eco-friendly, organic solvent-free and cost-effective hydrothermal method. These nanoparticles were used as a modifier of carbon paste electrodes (CPE), showing exceptional catalytic efficiency. Electrochemical measurements revealed that the developed electrode facilitates electron transfer processes and enhances the catalytic response. The resulting $Sm_2(MoO_4)_3$/CPE sensor exhibited a broad linear range of 0.1–100 and 100–300 μM of MTL, with low detection and quantification limits of 0.047 and 0.156 μM, respectively, at pH 3 in a Britton–Robinson buffer solution (BRBS) as the supporting electrolyte. The findings from the analysis of real water samples from various sources using this sensor were encouraging, suggesting that this method could offer a cost-effective, rapid and sensitive sensor for ambient MTL monitoring.

Keywords: environmental analysis; carbon paste electrode; organic pollutants; rare earth nanoparticles; electrochemical sensor.

INTRODUCTION

In photographic processes, photosensitive materials are used by photographers to convert latent images into visible ones.[1] Among other photographic

* Corresponding author. E-mail: dalibors@chem.bg.ac.rs
https://doi.org/10.2298/JSC240913102M

developers, metol (MTL) has been used as a monochrome photographic chemical for more than 100 years in Europe.[2,3] MTL, chemically *N*-methyl-*p*-aminophenol sulphate with formula $[HOC_6H_4NH_2(CH_3)]_2SO_4$, is also used as a corrosion inhibitor, antioxidant and antimicrobial agent, and it serves as an intermediary for the medication diloxanide and dyes for fur and hair.[4,5] Since it is used in the photographic industry, it is released into the water, contaminating ground, and household water.[6] It can be easily found in different water bodies such as rivers, lakes, ponds and seas.[1] MTL was found to be a cancerogenic organic pollutant with a significant impact on human health, the environment, animals, plants, and water sources.[7] MTL is non-biodegradable and can accumulate in biotic organisms. It is also related to numerous environmental issues, even in low concentrations.[2] Furthermore, a larger dose of MTL is necessary to have a substantial effect on several health problems, such as cancer, irritable eyes, slowed heartbeat, skin allergies and harm to the body's internal blood supply.[8] Therefore, developing a straightforward, quick, affordable, sensitive and practical method for MTL detection in aquatic bodies is imperative.

Various methods for MTL detection were reported, such as spectrophotometry,[9,10] ceric oximetry,[11] photolysis[12] and liquid chromatography–mass spectrometry.[7] Besides that, a few works using electroanalytical methods for MTL detection were reported.[13–15] Despite the incredible accuracy of these analytical techniques, they are costly, time-consuming, and require complex sample preparation procedures.[5,16] On the other hand, electrochemical methods have many advantages over conventional analytical techniques, such as low cost, ease of sample preparation, wide detection range, improved sensitivity and selectivity, facilitated device miniaturization, *in vivo* and *in vitro* process monitoring and they are user-friendly.[5,16–18] Several problems were solved with an electrode modification, such as slow electron transfer kinetics and gradual passivation of the surface, a higher transfer of electrons, enhanced conductivity, and surface area.[19] The application of modified electrodes as working in a three-electrode system for the electrochemical detection allows trace-level analysis[20,21] and increased the sensitivity of detection.[22]

In this work, $Sm_2(MoO_4)_3$ nanoparticles were synthesized using the hydrothermal method to modify the carbon paste electrode as a working electrode in electrochemical measurements. The morphological characteristics of synthesized material were investigated through X-ray diffraction (XRD), scanning electron microscope (SEM) and transmission electron microscope (TEM). The electrochemical properties of modified electrodes were studied by cyclic voltammetry (CV) and electrochemical impedance spectroscopy (EIS). differential pulse voltammetry (DPV) and square wave voltammetry (SWV) were compared and optimized for the selective and sensitive electrochemical detection of MTL. The real

sample application of the developed sensor was tested using the SWV method under the optimized working conditions.

EXPERIMENTAL

Materials and methods

All chemicals used in this study were purchased by Sigma Aldrich, which had the highest purity and were used without further purification. For $Sm_2(MoO_4)_3$ nanoparticles synthesis, samarium (III) nitrate hexahydrate ($Sm(NO_3)_3{\cdot}6H_2O$; 99.9 %), ammonium molybdate tetrahydrate ($(NH_4)_6Mo_7O_{24}{\cdot}4H_2O$; 99.98%), nitric acid (65 %), and ammonia solution (25 %) were used. The solution of analyte metol (4-(methylamino)phenol sulphate; ≥98.0 %) was freshly prepared before every measurement. As the supporting electrolyte, Britton–Robinson buffer solution (BRBS) was used (0.04 M mixture of boric acid, acetic acid and phosphoric acid) and pH value was adjusted by using the NaOH solution. The electrochemical characterization of electrodes was performed in 5 mM $Fe^{2+/3+}$ solution (potassium hexacyanoferrate (II) trihydrate ($K_4[Fe(CN)_6]{\cdot}3H_2O$ and potassium hexacyanoferrate (III) ($K_3[Fe(CN)_6]$) in 0.1 M KCl). The organic compound solutions (vitamins B6, B1, C, sucrose and glucose) were used to investigate potential interferents, and gallic acid, hydroquinone and bisphenol A solutions were used for the selectivity study. As a real sample, tap, and pond water were used.

Jeol JSM 7001 F (JEOL, Ltd., Japan) electron microscope was used for the analysis of the surface morphology of the $Sm_2(MoO_4)_3$ sample. Additionally, the Rigaku Optima IV powder diffractometer (Rigaku, Japan) was used for the examination of its phase composition and structure. The survey was recorded in the range of 2θ angles from 5 to 90° at a survey rate of 2°/min by using radiation from a CuKα copper tube (λ = 1.541 Å) at an accelerating voltage of 40 kV. The FTIR spectra of the sample, dispersed in KBr and compressed into pellets, were recorded using an FTIR Spectrometer Thermo Nicolet iS20 (Thermo Fisher Scientific) in the range of 4000–400 cm^{-1} at 64 scans per spectrum at 4 cm^{-1} resolution. The Raman spectra, excited with a diode-pumped solid-state high-brightness li laser (532 nm) were collected on a Thermo Scientific DXR Raman microscope (Thermo Fisher Scientific), equipped with a research optical microscope and CCD detector. The laser beam was focused on the sample placed on the *X*–*Y* motorized sample stage using objective magnification ×10. The scattered light was analyzed by the spectrograph with a grating of 900 lines mm^{-1}. The laser power was kept at 0.1 mW on the samples.

A PalmSens4 analyzer (Houten, Utrecht, The Netherlands) running PSTrace voltammetry software (version 5.8) was used for all electrochemical measurements. Unmodified and modified carbon paste electrodes were applied as working electrodes, Ag/AgCl was applied as the reference electrode, and a platinum wire was used as a counter electrode in a three-electrode system at room temperature.

Synthesis of $Sm_2(MoO_4)_3$ nanoparticles and electrodes preparation

Samarium (III) nitrate hexahydrate (0.1 mol; *Mr* = 444.47) and ammonium molybdate tetrahydrate (0.1 mol; *Mr* = 1235.86) were dissolved in 2 mL HNO_3 (2 M) and 2 mL deionized water at room temperature, followed by stirring. The pH value of the solution was adjusted to 6 using ammonia NH_3 solution (25 %). The solution was stirred for 30 min and then transferred to a hydrothermal autoclave for 24 h at 180 °C. The precipitate was filtrated, washed with water, ethanol and acetone, and dried overnight at room temperature.

A bare carbon paste electrode (CPE) was prepared by hand-mixing graphite powder and paraffin oil in a mass ratio of 70:30 (graphite powder/paraffin oil), in an agate mortar with a

pestle, until a homogenous paste was achieved. The obtained paste was pressed into a homemade Teflon electrode body with the inner diameter of 2 mm and smoothed on paper to get a uniform surface. The modified carbon paste electrodes were prepared following the same procedure, but with the addition of different percentages of synthesized material. $Sm_2(MoO_4)_3$ nanoparticles were added to paste in 5, 10, 15 and 20 wt. %.

RESULTS AND DISCUSSION

Morphological properties of synthesized $Sm_2(MoO_4)_3$ nanoparticles

The SEM images of $Sm_2(MoO_4)_3$ are presented in Fig. 1A and B, recorded at different sizes of magnitudes. Namely, the aggregated granular-like morphology was obtained for $Sm_2(MoO_4)_3$. A similar kind of morphology of $Sm_2(MoO_4)_3$ was obtained by S. Behvandi *et al.*[23] The EDS spectrum of $Sm_2(MoO_4)_3$ confirmed the presence of Sm, Mo and O elements in Fig. 1C. The mapping images of Sm, Mo and O exhibited their uniform distribution.

Fig. 1D shows the XRD pattern of the $Sm_2(MoO_4)_3$ which contains the diffraction peaks at 28.65, 34.04 and 46.74° corresponding to the reflection from (111), (221) and (100) crystal planes of $Sm_2(MoO_4)_3$.[23–25] These obtained results confirmed the good crystallinity[26] of the synthesized sample. Irrespective of its environment, the stretching and bending internal modes of the molybdate ion appear in the region 950–775 cm^{-1} and 425–275 cm^{-1}, respectively. On the other hand, the frequency of the external modes strongly depends on the nature of the cation.[27] Fig. 1E shows the FTIR spectrum of the $Sm_2(MoO_4)_3$. All the ν_1 and ν_3 stretching vibrational modes fall in the broad contour from 1000 to 600 cm^{-1}.[27] The bending region shows one band centred at 429 cm^{-1}.[27] In the Raman spectrum, Fig. 1F, one can see that the modes are observed in two well-separated regions, *i.e.*, 1000–700 and 400–300 cm^{-1}. The bands located below 300 cm^{-1} are attributed to external vibrations of the MoO_4 anions and translational modes of cations.[28]

All of these results confirmed that the synthesized sample is samarium molybdate.[23]

Electrochemical properties of the prepared electrode

EIS and CV were used for electrochemical investigations of the prepared electrodes in 5 mM $[Fe(CN)_6]^{3-/4-}$ and 0.1 M KCl solution. Fig 2A shows Nyquist plots observed for bare CPE and 5,10, 15 and 20 wt. % modified carbon paste electrodes. A straight line can be seen in the low-frequency part of the graph, which is related to the diffusion transfer of ions into the electrode material (Warburg diffusion). In contrast, a semicircle can be seen in the high-frequency zone, corresponding to the charge transfer process.[29] The *Rct* value is the diameter of the semicircle, representing the quantitative measure of the resistance to charge transfer.[29] The electrochemical performance of the electrode is strongly related to the *Rct* value.[30,31] The *Rct* value of the 15 wt. % modified electrode is 285.5 Ω, and

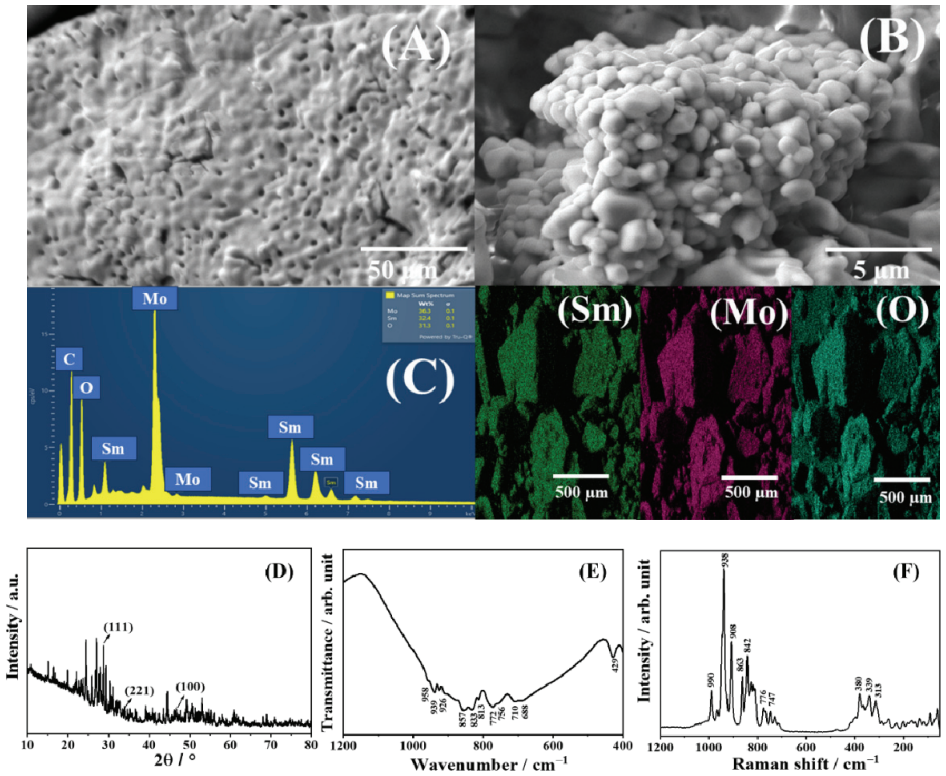

Fig. 1. A, B) SEM images of $Sm_2(MoO_4)_3$ at different magnifications with the corresponding EDS spectrum (C) and mapping images of Sm, Mo and O; D) XRD pattern; E) FTIR and F) Raman spectra of $Sm_2(MoO_4)_3$.

it is lower compared to the *Rct* values of bare CPE and 5, 10 and 20 wt. % modified electrodes, which *Rct* values are 3647.9, 313.5, 430.8 and 367.1 Ω, respectively. Much lower charge transfer resistance of the 15 wt. % modified CPE indicates that $Sm_2(MoO_4)_3$ nanoparticles efficiently promote the electron transfer processes, increasing the flow rate of ferricyanide species toward the electrode surface. These results confirm that the electron transfer kinetics of the modified electrode is quite excellent. From the straight line in the low-frequency plots, the diffusion coefficient could be estimated using the following equation:[31]

$$D = (RT)^2/(2A^2n^4F^4C^2\sigma^2) \quad (1)$$

where R is the universal gas constant (8.314 J mol^{-1} K^{-1}), T corresponds to temperature (K), A denotes electroactive surface area (cm^2), n is the number of electrons transferred, F symbolizes Faraday constant (96485 C mol^{-1}), C is the concentration, and σ is the Warburg factor related to Z'. The Warburg factor σ could be obtained by linearly fitting the relationship curve between Z' and the angular

frequency reciprocal square root, shown for all electrodes in Fig. S-1 of the Supplementary material to paper.

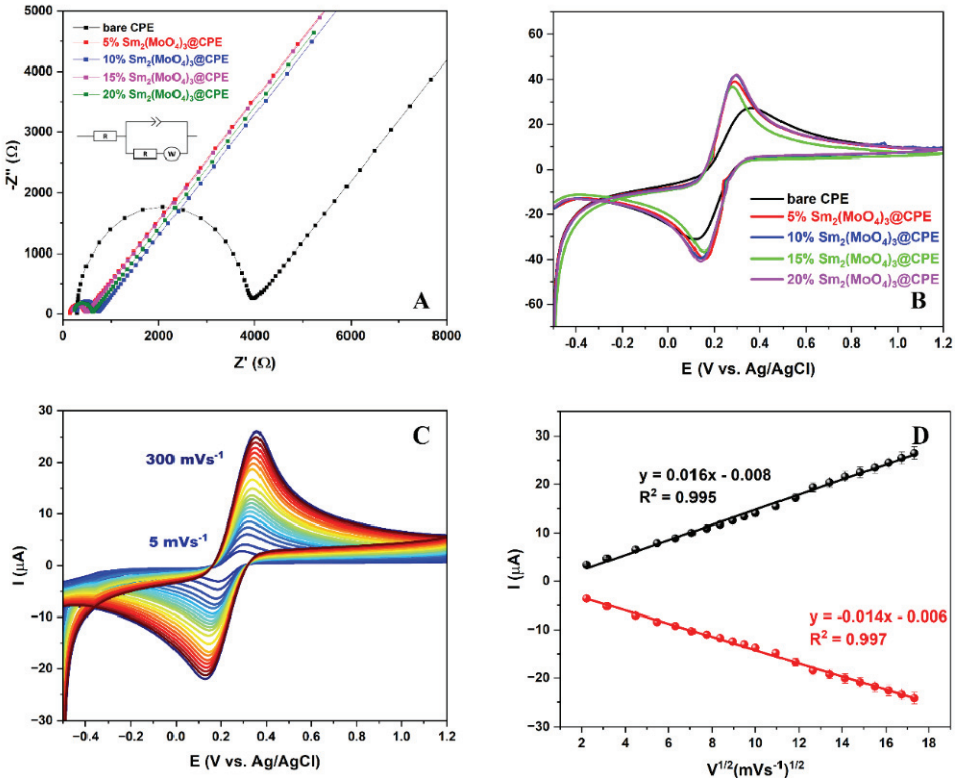

Fig. 2. A) Nyquist plots and B) CV studies of bare CPE and 5, 10, 15 and 20 wt. % modified CPEs in 5 mM $[Fe(CN)_6]^{3-/4-}$ and 0.1 M KCl solution; C) CV curves of 15 wt. % modified CPE at different scan rates in a range from 5 to 300 mV s^{-1}; D) dependence of redox peak currents on the square root of the scan rate.

In the same solution, CV measurements were performed in the potential range from –0.5 to 1.2 V. As shown in Fig. 2B, redox peak currents of bare CPE (27.29 μA for oxidation and –34.05 μA for reduction) are much lower when compared to 5, 10, 15 and 20 wt. % modified electrodes whose peak currents are 40.82, 46.18, 41.98 and 47.46 μA for oxidation, respectively, and –40.62, –42.33, –39.76 and –45.56 μA for reduction, respectively. The 15 wt. % modified electrode showed the lowest peak-to-peak separation value (ΔE = 0.120V) compared to bare CPE, 5, 10 and 20 wt. % modified electrodes with values of 0.232, 0.141, 0.151 and 0.157 V, respectively. For all prepared electrodes, the electrochemical behavior of $Fe^{2+/3+}$ at different scan rates was investigated and presented in Fig. S-2 of the Supplementary material. Fig. 2C shows the impact of the scan rate on

redox peaks of $Fe^{2+/3+}$ over 15 wt. % modified CPE. With increasing scan rate, the redox peak currents also increase with the linear dependence of redox peak currents on the square root of the scan rate, shown in Fig. 2D, and this dependence for all other electrodes is shown in Fig. S-3 of the Supplementary material. From these results, the electroactive surface areas of all electrodes were calculated using the Randles–Sevcik equation:[32]

$$I_p = 2.69\times10^5 n^{3/2} A D^{1/2} C V^{1/2} \quad (2)$$

where I_p is peak current (A), n denotes transferred electrons, D signifies diffusion coefficient ($cm^2\ s^{-1}$), C is the concentration of solution (mol cm^{-3}), and V is the scan rate ($V\ s^{-1}$). All of the modified electrodes have higher values of the electroactive surface area than the bare CPE, indicating that incorporating synthesized material into the carbon paste improved the electron transport capacity and accelerated the electron transfer rates. All calculated values are presented in Table S-I of the Supplementary material. Considering all mentioned above, the electrode with a 15 wt. % modifier was chosen for further electrochemical measurements.

Detection of MTL and optimization of pH of the supporting electrolyte

The CV measurements (Fig. 3A) were performed in 100 μM MTL solution in BRBS pH 3 as supporting electrolyte over bare carbon paste electrode and 15 wt. % $Sm_2(NO_3)_3$ modified electrode, since it showed the best electrocatalytic behaviour in $Fe^{2+/3+}$ solution. The modified electrode shows better MTL response with peak currents of 5.37 μA for the oxidation and –5.33 μA for the reduction than bare CPE, whose peak values are 5.00 and –4.90 μA for the oxidation and the reduction, respectively. A lower value of peak-to-peak separation was obtained with modified CPE, 59 mV, compared to bare CPE, 67 mV. These results indicate that the $Sm_2(NO_3)_3$ modified electrode has outstanding electrocatalytic activity and a quick electron transfer mechanism.

A significant role in developing sensitive and selective sensor plays the pH value of supporting electrolyte. Fig. 3B represents cyclic voltammograms of 100 μM MTL solution at 50 mV s^{-1} at different pH values of BRBS, in the range from 2 to 9. With the increasing pH value of the supporting electrolyte, a significant potential shift to lower values can be seen. This shifting is linear, and the relationship between potential and pH values is presented in Fig. 3C. The dependence of peak potential on pH value is linear for the oxidation and reduction processes with the equations: $y = -0.062x + 0.565$ and $y = -0.064x + 0.517$ with linear regression coefficients R^2 0.993 and 0.996, respectively. Since the slopes of curves are 62 and 65 mV, and both are very close to the theoretical value of 59 mV, it was proved that the mechanism of oxidation involves an equal number of electrons and protons (m/n), using the following equation:[2]

$$E_p = (0.059m/n)\text{pH} + b \quad (4)$$

Fig. 3D represents the relationship between the supporting electrolyte's peak current and pH value. For both oxidation and reduction processes, the highest peak current of the signal was obtained on pH 3, which is selected for all further measurements.

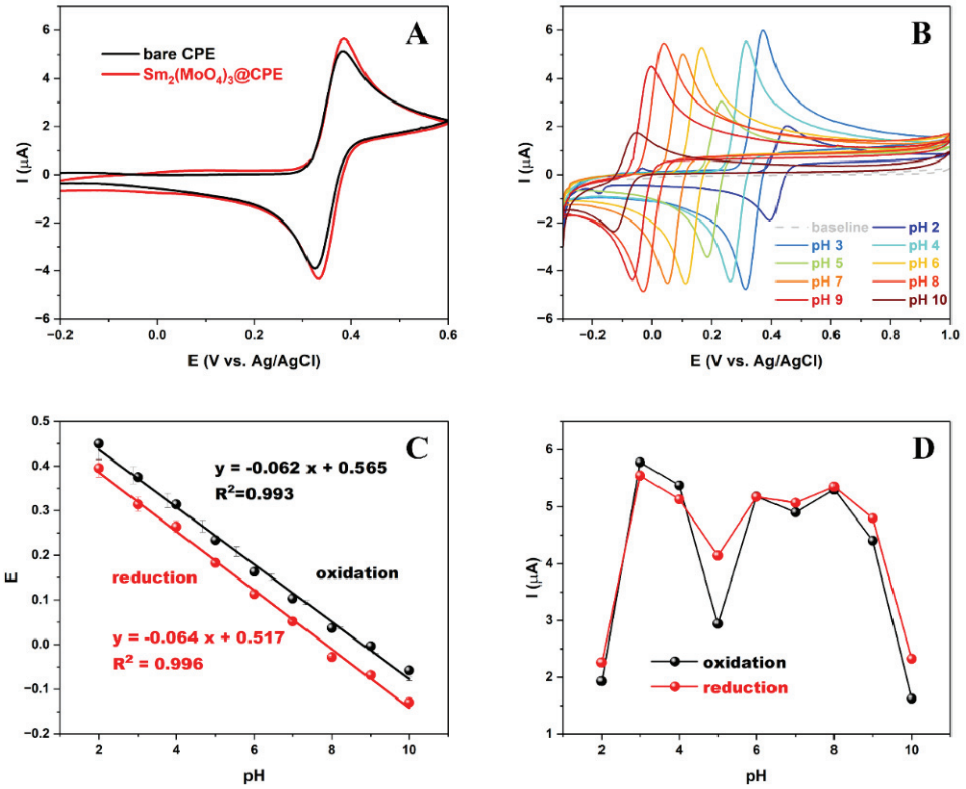

Fig. 3. A) Cyclic voltammogram (CV) of bare carbon paste electrode and 15 wt. % $Sm_2(MoO_4)_3$ modified electrode in 100 μM MTL solution at pH 3; B) CV measurements of 100 μM MTL solution at 50 mV s^{-1} at different pH values of BRBS in the range from 2 to 9; C) dependence of peak potential on pH value of supporting electrolyte in the range from 2 to 9; D) dependence of peak current on pH value of supporting electrolyte in the range from 2 to 9.

Electrochemical behavior of MTL at different scan rates over $Sm_2(MoO_4)_3$/CPE sensor

The electrochemical behaviour of MTL was investigated through CV measurements at different scan rates ranging from 2 to 300 mV s^{-1} in 100 μM MTL solution over a 15 wt. % modified $Sm_2(MoO_4)_3$/CPE electrode. As shown in Fig. 4A, the peak current increases with the scan rate values, implying that the redox reaction of MTL is scan rate dependent. This relationship is shown in Fig. 4B for

both oxidation and reduction peaks. The dependence of redox peak currents is linear on the square root of the scan rate with equations $y = 0.763x - 0.071$ with R^2 0.999 and $y = -0.857x + 0.619$ with R^2 0.999 for the oxidation and the reduction, respectively, indicating that the MTL redox reaction is a diffusion-controlled process. This statement was also proved by the linear dependence of log I on $log\ V$ (Fig. 4C) with a slope of 0.499 for the oxidation and –0.502 for the reduction peak, which is very close to the theoretical slope of 0.5 for diffusion--controlled processes.[8] Furthermore, the redox peak potential is linearly dependent on the natural logarithm of the scan rate (Fig. 4D) and the linear regression plot as $y = 0.031x + 0.347$ with R^2 0.96, and $y = -0.029x + 0.354$ with R^2 0.90 for oxidation and reduction, respectively. The number of electrons participating in the MTL redox reaction was calculated using the following equations:[34]

$$E_p = E_0' + (2.303RT/\alpha nF)\log(RTk_0/\alpha nF) + (2.303RT/\alpha nF)\log V \quad (5)$$

$$E_{p/2} - E_p = 1.857RT/\alpha F \quad (6)$$

where α, k_0, n, V, E_0' and $E_{p/2}$ are the transfer coefficient, the standard heterogeneous rate constant of the reaction, the number of electrons, scan rate, formal

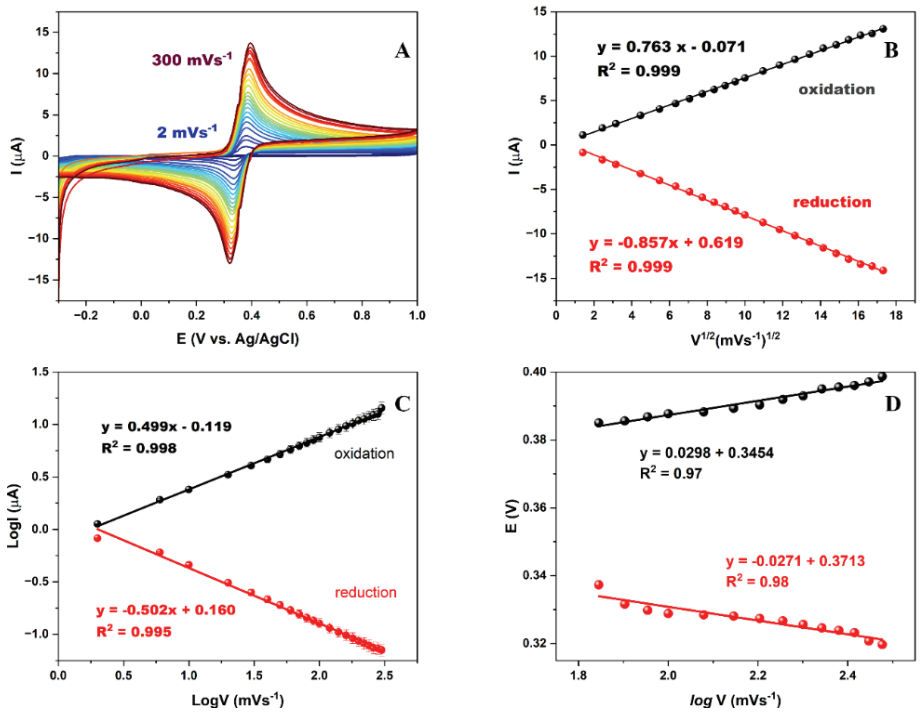

Fig. 4. A) CV curves of the 100 μM MTL solution over 15 wt. % modified CPE at different scan rates in a range from 2 to 300 mV s^{-1}; B) the dependence of the redox peak currents on the square root of the scan rate; C) dependence of the log I on the log V for redox peaks; D) dependence of the potential value on the logV for redox peaks.

redox potential and the potential when the current is at half of the peak value, respectively. Other symbols have their common meanings. The values of α and n are calculated to be 0.4072 and 2.3, which is close to 2. The mechanism of the MTL redox reaction was confirmed with everything mentioned above, where two electrons and two protons participate in this reaction, which follows previously reported works.

Quantification of MTL

The pulse methods were tested to develop sensitive and selective methods for quantification of MTL. We compared DPV and SWV, and the comparison between these two techniques is shown in Fig. 5A. The obtained peak currents with SWV are 15.37 and 15.70 μA for the oxidation and the reduction, respectively, while the values achieved using the DPV method are 6.97 and 6.93 μA for the oxidation and the reduction, respectively. Comparing peaks, a well-shaped peak is obtained using the SWV method, with higher peak currents for the oxid-

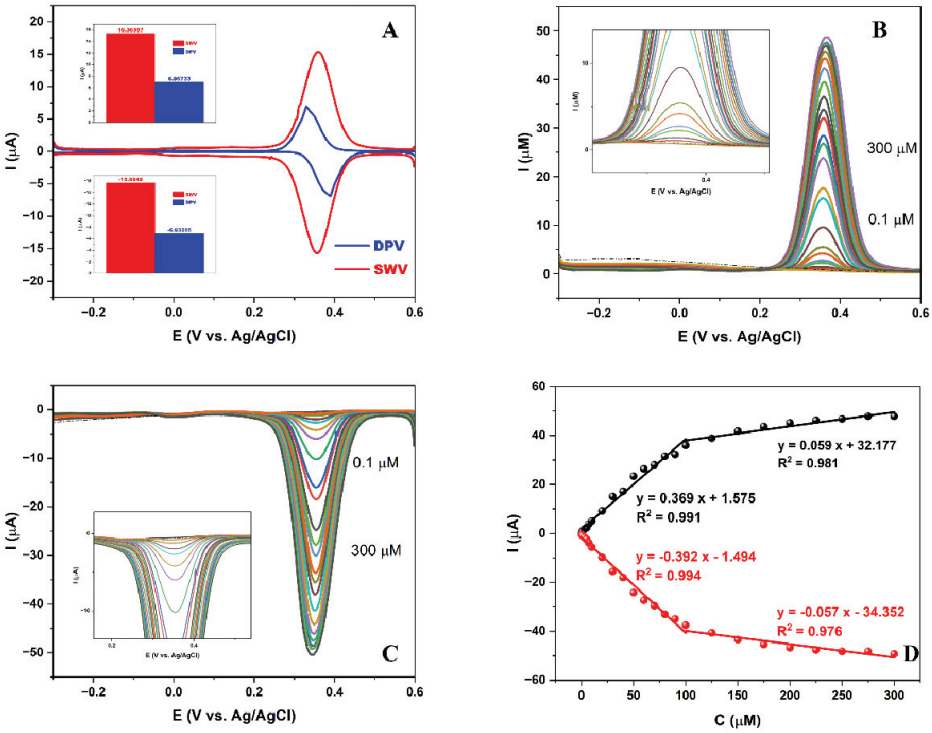

Fig. 5. A) Voltammograms of 100 μM MTL solution in BRBS at pH 3 obtained using DPV and SWV methods; B) anodic peak of the 15 wt. % $Sm_2(MoO_4)_3$ modified electrode at different concentrations of MTL in BRBS at pH 3; C) cathodic peak of the 15 wt. % $Sm_2(MoO_4)_3$ modified electrode at different concentrations of MTL in BRBS at pH 3; D) calibration plot derived from SWV measurements as a function of MTL concentration.

ation and the reduction. Considering all the above, the SWV method was optimized and applied for MTL quantification. The working parameters are optimized and shown in Fig. S-4 of the Supplementary material. The chosen values for further measurements were 30 mV for amplitude and 10 Hz for frequency. Under the optimized parameters, the effect of higher concentrations of MTL on peak current was investigated, shown in Fig. 5B for the oxidation and Fig. 5C for the reduction peak. The measurements were performed at a potential range from –0.3 to 0.6 V, with the addition of MTL solution from 0.1 to 300 μM. The relationship between peak currents and MTL concentrations is shown in Fig. 5D. The dependence of the peak current on the concentration of MTL is linear in two regions: from 0.1 to 100 μM with equations $y = 0.369x + 1.575$ and R^2 0.99 for oxidation and $y = –0.392x – 1.494$ with R^2 0.99 for reduction and from 100 to 300 μM with equations $y = 0.059x + 32.177$ with R^2 0.98 for oxidation and $y = = –0.057x – 34.352$ with R^2 0.98 for reduction. The limit of detection (*LOD*) and limit of quantification (*LOQ*) for the developed method were calculated as 3σ/S and 10σ/S, respectively, where σ signifies the blank's standard deviation, and *S* stands for the calibration curve's slope. *LOD* for oxidation is 0.059 and 0.047 μM for reduction, and *LOQ* values are 0.196 and 0.156 μM for the oxidation and the reduction, respectively. The sensitivity of the developed sensor was calculated as the slope/surface area of the electrode, and the values are 76.01 μA μM^{-1} cm^{-2} for the oxidation and 80.63 μA μM^{-1} cm^{-2} for the reduction. Table S-II of the Supplementary material compares the prepared $Sm_2(MoO_4)_3$/CPE sensor to the other differently modified electrodes.

Interference and selectivity study

A 100 μM solution of MTL and 100 μM of vitamins B6, B1, C, sucrose and glucose were prepared for interference measurements. The SWV measurements were performed under optimized working parameters ranging from –0.3 to 0.6 V (Fig. S-5 of the Supplementary material). All of the species had less than 5 % influence on the peak of MTL, besides glucose, which is considered a potential interferent for MTL detection. The selectivity study was performed with 100 μM solutions of other phenolic compounds, such as gallic acid, hydroquinone (HQ), and bisphenol A. The results of SWV measurements of 100 μM solution of MTL with the addition of phenolic compounds were shown in Fig. S-6 of the Supplementary material. Neither of the tested phenolic compounds significantly impacted MTL redox peak currents, which means that the developed sensor can be used as an excellent tool for MTL detection in real samples.

Real samples application

A developed sensor for sensitive and selective MTL detection and quantification was employed in tap and pond water. SWV measurements were per-

formed in a potential range from –0.3 to 0.6 V. The pH values of the real samples were adjusted using BRBS pH 3, and the measured pH values of the real samples were 3.09 and 3.11 for tap water and pond water, respectively. Fig. 6A and B represents voltammograms of the real sample solutions and the solutions with spiked 5, 10, 15 and 20 μM concentrations of MTL. Added and found concentrations of MTL are given in Table I for both real samples and for the determination in both oxidation and reduction processes. According to the findings of these real-world sample investigations, the $Sm_2(MoO_4)_3$ modified carbon paste electrode shows excellent precision and reliability regarding the real-time MTL detection from water samples.

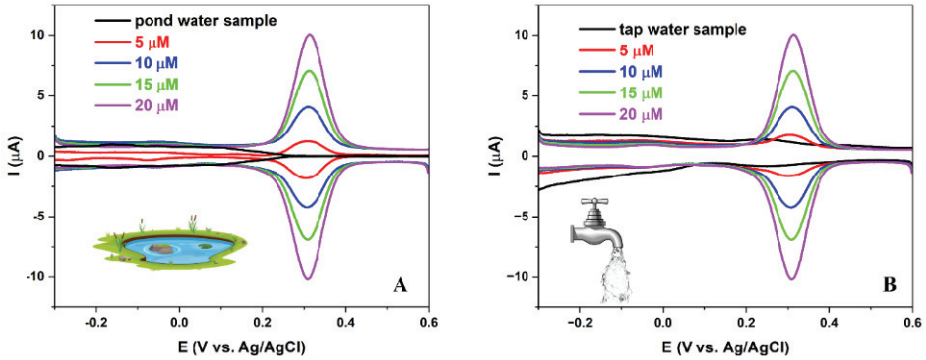

Fig. 6. SWV measurements of: A) pond water sample and B) tap water sample, with spiked 5, 10, 20 and 25 μM of MTL.

TABLE I. Real sample analysis of MTL in pond water and tap water samples

Sample	Added μM	Found μM	Recovery %	Reduction	Added μM	Found μM	Recovery %
Tap water	4.97	4.94	99.40	Tap water	4.97	4.66	93.76
	9.90	9.82	99.19		9.90	9.94	100.40
	14.78	14.86	100.54		14.78	14.79	100.07
	19.61	19.41	98.98		19.61	20.14	102.70
Pond water	4.97	4.95	99.60	Pond water	4.97	4.63	93.16
	9.90	9.76	98.59		9.90	9.82	99.19
	14.78	14.98	101.35		14.78	14.84	100.41
	19.61	19.47	99.29		19.61	20.41	104.08

CONCLUSION

To conclude, we developed a very efficient technique for detecting and quantifying the nitrogen-organic pollutant metol by employing samarium molybdate nanomaterial as a modifier for the carbon paste electrode. We carefully evaluated the morphological characteristics of the nanomaterial using methods including TEM, SEM and XRD. With a detection and quantification limit of 0.047

and 0.156 μM and a wide linear range of 0.1–100 and 100–300 μM, the SWV method over the fabricated electrodes showed remarkable results. Since real sample analyses, such as those of tap and pond water, gave excellent results, this improved method can be easily applied in everyday research.

SUPPLEMENTARY MATERIAL

Additional data and information are available electronically at the pages of journal website: https://www.shd-pub.org.rs/index.php/JSCS/article/view/13044, or from the corresponding author on request.

Acknowledgement. This work was financially supported by the Ministry of Science, Technological Development and Innovation of Republic of Serbia, contracts No: 451-03-66/ /2024-03/200168 and 451-03-66/2024-03/200026.

И З В О Д

ОДРЖИВА СИНТЕЗА НАНОЧЕСТИЦА САМАРИЈУМ-МОЛИБДАТА: ЈЕДНОСТАВАН ЕЛЕКТРОХЕМИЈСКИ АЛАТ ЗА ДЕТЕКЦИЈУ ЗАГАЂИВАЧА ЖИВОТНЕ СРЕДИНЕ МЕТОЛА

ТИЈАНА МУТИЋ[1], ВЕСНА СТАНКОВИЋ[2], ЈАДРАНКА МИЛИКИЋ[2], ДАНИЦА БАЈУК-БОГДАНОВИЋ[2], KURT KALCHER[3], ASTRID ORTNER[4], ДРАГАН МАНОЈЛОВИЋ и ДАЛИБОР СТАНКОВИЋ[5]

[1]Универзитет у Београду, Институт за хемију, технологију и металургију, Његошева 12, 11000 Београд, [2]Универзитет у Београду, Факултет за физичку хемију, Студентски трг 12–16, 11158 Београд, [3]Institute of Chemistry, Analytical Chemistry, Karl-Franzens University, Universitaetsplatz I/I, 8010 Graz, Austria, [4]University of Graz, Institute of Pharmaceutical Sciences, Department of Pharmaceutical Chemistry, Schubertstraße 1, 8010 Graz, Austria и [5]Универзитет у Београду, Хемијски факултет, Студентски трг 12–16, 11158 Београд

Ова студија је фокусирана на развој високо ефикасног сензора за детекцију и квантификацију органског загађивача метола. У ту сврху, наночестице самаријум-молибдата су синтетисане применом еколошки прихватљиве и јефтине хидротермалне методе, без коришћења органских растварача. Ове наночестице су примењене као модификатор електрода од угљеничне пасте због своје изузетне каталитичке ефикасности. Електрохемијска мерења су открила да развијен сензор олакшава процесе преноса електрона и побољшава каталитички одговор електроде. Добијени сензор је показао широк линеарни опсег од 0,1–100 и 100–300 μM метола, са ниским границама детекције и квантификације од 0,047 и 0,156 μM, редом, при pH 3 у Бритон–Робинсоновом пуферском раствору као помоћном електролиту. Анализом реалних узорака воде из различитих извора помоћу овог сензора добијени су задовољавајући резултати, што сугерише да би овај сензор могао да се примењује у рутинским анализама, као брз, исплатив и осетљив метод.

(Примљено 13. септембра, ревидирано 7. октобра, прихваћено 2. децембра 2024)

REFERENCES

1. S. S. Rex Shanlee, R. Sundaresan, S. M. Chen, R. Balaji, T. Jeyapragasam, J. Y. Peng, A. I. Jothi, *Surf. Interf.* **40** (2023) 103020 (https://doi.org/10.1016/j.surfin.2023.103020)
2. K. Venkatesh, B. Muthukutty, S. M. Chen, P. Karuppasamy, A. S. Haidyrah, C. Karuppiah, C. C. Yang, S. K. Ramaraj, *J. Ind. Eng. Chem.* **106** (2022) 287 (https://doi.org/10.1016/j.jiec.2021.11.005)

3. W. Sun, Q. Jiang, Y. Wang, K. Jiao, *Sensors Actuators, B* **136** (2009) 419 (https://doi.org/10.1016/j.snb.2008.10.003)
4. X. Niu, L. Yan, X. Li, A. Hu, C. Zheng, Y. Zhang, W. Sun, *Int. J. Electrochem. Sci.* **11** (2016) 1720 (https://doi.org/10.1016/S1452-3981(23)15955-4)
5. K. Mariappan, S. Sakthinathan, S.-M. Chen, S. Alagarsamy, T.-W. Chiu, *J Electrochem. Soc.* **170** (2023) 126505 (https://doi.org/10.1149/1945-7111/ad1551)
6. S. Samanta, R. Srivastava, *J. Electroanal. Chem.* **777** (2016) 48 (https://doi.org/10.1016/j.jelechem.2016.07.024)
7. L. Lunar, *Water Res.* **34** (2000) 3400 (https://doi.org/10.1016/S0043-1354(00)00089-0)
8. C. Koventhan, V. Vinothkumar, S.-M. Chen, T.-W. Chen, A. Sangili, K. Pandi, V. Sethupathi, *Int. J. Electrochem. Sci.* **15** (2020) 7390 (https://doi.org/10.20964/2020.08.43)
9. C. S. P. Sastry, T. E. Divakar, U. Viplava Prasad, *Talanta* **33** (1986) 164 (https://doi.org/10.1016/0039-9140(86)80034-0)
10. R. R. Krishna, C. S. P. Sastry, *Fresenius' Zeitsch. Anal. Chem* **296** (1979) 46 (https://doi.org/10.1007/BF00481172)
11. W. Sun, Q. Jiang, K. Jiao, *J. Solid State Electrochem.* **13** (2009) 1193 (https://doi.org/10.1007/s10008-008-0646-8)
12. R. Andreozzi, *Water Res.* **34** (2000) 463 (https://doi.org/10.1016/S0043-1354(99)00183-9)
13. X. Hu, J. Qian, J. Yang, X. Hu, Y. Zou, N. Yang, *J. Electroanal. Chem.* **947** (2023) 117756 (https://doi.org/10.1016/j.jelechem.2023.117756)
14. M. M. Stanley, A. Sherlin V, S.-F. Wang, B. Sriram, J. N. Baby, M. George, *J. Environ. Chem. Eng.* **11** (2023) 110185 (https://doi.org/10.1016/j.jece.2023.110185)
15. B. Mutharani, P. K. Gopi, S.-M. Chen, H.-C. Tsai, F. Ahmed, A. S. Haidyrah, P. Ranganathan, *Ecotoxicol. Environ. Saf.* **220** (2021) 112373 (https://doi.org/10.1016/j.ecoenv.2021.112373)
16. K. Mariappan, D. D. F. Packiaraj, T.-W. Chen, S.-M. Chen, S. Sakthinathan, S. V. Alagarsamy, A. M. Al-Mohaimeed, W. A. Al-onazi, M. S. Elshikh, T.-W. Chiu, *New J. Chem.* **48** (2024) 6438 (https://doi.org/10.1039/D3NJ06004G)
17. F. Packiaraj Don Disouza, S. Alagarsamy, T.-W. Chen, S.-M. Chen, W.-C. Liou, B.-S. Lou, W. A. Al-onazi, M. Ajmal Ali, M. S. Elshikh, *J. Ind. Eng. Chem.* **135** (2024) 406 (https://doi.org/10.1016/J.JIEC.2024.01.052)
18. T. Mutić, D. Stanković, D. Manojlović, D. Petrić, F. Pastor, V. V. Avdin, M. Ognjanović, V. Stanković, *Electrochem.* **5** (2024) 45 (https://doi.org/10.3390/electrochem5010003)
19. N. Nataraj, T.-W. Chen, S.-M. Chen, T. Kokulnathan, F. Ahmed, T. Alshahrani, N. Arshi, *J. Taiwan Inst. Chem. Eng.* **156** (2024) 105348 (https://doi.org/10.1016/j.jtice.2024.105348)
20. S. Knežević, M. Ognjanović, V. Stanković, M. Zlatanova, A. Nešić, M. Gavrović-Jankulović, D. Stanković, *Biosensors (Basel)* **12** (2022) 705 (https://doi.org/10.3390/bios12090705)
21. M. Ognjanović, D. M. Stanković, Ž. K. Jaćimović, M. Kosović-Perutović, J. F. M. L. Mariano, S. Krehula, S. Musić, B. Antić, *Electroanalysis* **34** (2022) 1431 (https://doi.org/10.1002/elan.202100602)
22. T. Mutić, M. Ognjanović, I. Kodranov, M. Robić, S. Savić, S. Krehula, D. M. Stanković, *Anal. Bioanal. Chem.* **415** (2023) 4445 (https://doi.org/10.1007/s00216-023-04617-70
23. S. Behvandi, A. Sobhani-Nasab, M. A. Karimi, E. Sohouli, M. S. Karimi, M. R. Ganjali, F. Ahmadi, M. Rahimi-Nasrabadi, *Polyhedron* **180** (2020) 114424 (https://doi.org/10.1016/j.poly.2020.114424)

24. K. P. Mani, V. G., P. R. Biju, C. Joseph, N. V. Unnikrishnan, M. A. Ittyachen, *ECS J. Solid State Sci. Technol.* **4** (2015) R67 (https://doi.org/10.1149/2.0131505jss)
25. Z. Rezapoor-Fashtali, M. R. Ganjali, F. Faridbod, *Biosensors (Basel)* **12** (2022) 720 (https://doi.org/10.3390/bios12090720)
26. M. V. Raskina, V. A. Morozov, A. V. Pavlenko, I. G. Samatov, I. V. Arkhangel'Skii, S. Stefanovich, B. I. Lazoryak, *Russ. J. Inorg. Chem.* **60** (2015) 84 (https://doi.org/10.1134/S0036023615010118)
27. S. S. Saleem, G. Aruldhas, H. D. Bist, *Spectrochim. Acta, A* **39** (1983) 1049 (https://doi.org/10.1016/0584-8539(83)80124-X)
28. W. Dridi, M. F. Zid, M. Maczka, *Adv. Mat. Sci. Eng.* **2017** (2017) 1 (https://doi.org/10.1155/2017/6123628)
29. Z. Zhang, X. Liu, Y. Wu, H. Zhao, *J. Solid State Electrochem.* **19** (2015) 469 (https://doi.org/10.1007/s10008-014-2624-7)
30. H. Zhao, B. Chen, C. Cheng, W. Xiong, Z. Wang, Z. Zhang, L. Wang, X. Liu, *Ceram. Int.* **41** (2015) 15266 (https://doi.org/10.1016/j.ceramint.2015.07.213)
31. H. Zhao, N. Hu, R. Xu, H. Liu, J. Liu, Q. Ran, *Ceram. Int.* **46** (2020) 21805 (https://doi.org/10.1016/j.ceramint.2020.05.256)
32. V. Stanković, S. Đurđić, M. Ognjanović, G. Zlatić, D. Stanković, *Sensors* **24** (2024) 705 (https://doi.org/10.3390/s24020705)
33. V. C. Valsalakumar, S. Vasudevan, *Langmuir* **39** (2023) 15730 (https://doi.org/10.1021/acs.langmuir.3c02303)
34. A. Afkhami, F. Soltani-Felehgari, T. Madrakian, H. Ghaedi, *Biosens. Bioelectron.* **51** (2014) 379 (https://doi.org/10.1016/j.bios.2013.07.056)
35. S. P. Thangavelu, T.-W. Chen, S.-M. Chen, K. Thangavelu, B.-S. Lou, T. saad Algarni, W. A. Al-onazi, M. S. Elshikh, *Carbon N.Y.* **223** (2024) 119026 (https://doi.org/10.1016/j.carbon.2024.119026)
36. S. Alagarsamy, R. Sundaresan, T.-W. Chen, S.-M. Chen, B.-S. Lou, B. Ramachandran, S. K. Ramaraj, M. Ajmal Ali, M. S. Elshikh, J. Yu, *Microchem. J.* **193** (2023) 108960 (https://doi.org/10.1016/j.microc.2023.108960)
37. S. Jose, A. George, A. R. Cherian, A. Varghese, *Surfaces Interf.* **35** (2022) 102416 (https://doi.org/10.1016/j.surfin.2022.102416).